Synoptic and microphysical lifetime constraints for contrails

Sina Maria Hofer[1] and Klaus Martin Gierens[1]

[1]Deutsches Zentrum für Luft- und Raumfahrt, Institut für Physik der Atmosphäre, Oberpfaffenhofen, Germany

Correspondence: Sina Maria Hofer (sina.hofer@dlr.de)

Abstract.

Contrail lifetime is constrained mainly by the sedimentation of ice crystals into lower levels that are subsaturated, the blowing out of the ice crystals from the parent ice supersaturated regions (ISSRs) by the (horizontal) wind~~,~~ and the reduction of supersaturation down to subsaturation due to large-scale subsidence. The first of these processes can be characterised by a sedimentation time-scale. The second and third processes can together be characterised by a synoptic time-scale. The synoptic time-scale is determined in this paper with trajectory calculations for air parcels that initially reside in ice supersaturated regions and which either leave these with the wind or where the ice supersaturation itself vanishes. It is crucial to know the time-scales of contrails because their individual effect on climate depends on their lifetime. The distinction between the two time-scales is particularly important for planning flights with alternative fuels for ~~the purpose of~~ the mitigation of contrail effects. This works in particular if sedimentation is the predominant contrail termination process, that is, if the sedimentation time-scale is shorter than the synoptic one. Here we show that both time-scales are of the order of a few hours. Actually, in nature, the three mentioned processes act simultaneously. The combined time-scale is half of the harmonic mean of the two time-scales in separation. Furthermore, we found as a side result that ISSRs only emerge in areas where the normalised geopotential height, Z^*, is ~~mainly~~ at least 0.98. For contrail-avoiding flight planning this means that contrail avoidance in regions with $Z^* < 0.98$ is ~~mainly~~ not necessary.

1 Introduction

The individual radiative effect of a contrail (instantaneous radiative forcing or energy forcing) is the radiative flux change (infrared and solar radiation) ~~which~~ that it causes during its complete lifetime. The lifetime of a single contrail is thus an important characteristic. Contrail lifetimes vary widely; most contrails are short and terminate already after a few minutes. These are contrails that have been formed under subsaturated conditions, ~~in air with subsaturated water vapour,~~ that is, where the relative humidity with respect to ice is below 100%. (We usually label such situations conveniently "subsaturated air", although it is not the air that is subsaturated, but the water vapour it contains.) Ice crystals in such an environment sublimate quickly. The contrail lifetime can be as short as a few seconds in very dry air up to a few minutes in slightly subsaturated air (Sussmann and Gierens, 2001). Such contrails are generally considered not climate-relevant. Contrails that are formed within ice supersaturated regions (ISSRs) become older than a few minutes. In fact, they can reach lifetimes exceeding 10 ~~hrs~~ h (e.g. Minnis et al., 1998; Haywood et al., 2009). These contrails are persistent and they can spread and extend into contrail-cirrus.

They are relevant for climate due to their interaction with radiation (Schumann et al., 2012; Wolf et al., 2023) and with nearby natural cirrus clouds (Verma and Burkhardt, 2022) and due to their effect on the upper-tropospheric water budget (Schumann et al., 2015). All these effects accumulate should get stronger with increasing contrail lifetime and thus it is important to consider the lifetime statistics from different viewpoints. Gierens and Vázquez-Navarro (2018) used contrail tracking data from a geostationary satellite to derive lifetime statistics. Taking into account unseen periods of contrail lifetimes, they derived a mean lifetime of the order of three hours and concluded that about 5% of contrails have lifetimes exceeding 10 hours.

Contrail lifetimes are mainly constrained by three different processes, one of which is known as the microphysical pathway, while the two others form the synoptic pathway (Bier et al., 2017). In the microphysical pathway, contrails are dissolved by sedimentation of their ice crystals into lower drier layers. The synoptic pathway implies that either the air itself which contains the contrail becomes drier and subsaturated or that the contrail is blown out of the ISSRs with the wind. Currently, it is unknown which of these pathways dominates or if they occur with similar frequency. This question, however, has some bearing on the use of alternative fuels in a given situation. Alternative fuels generally lead to reduced soot emission (Moore et al., 2017; Voigt et al., 2021), which in turn leads to less fewer but larger ice crystals which that sediment faster. This is beneficial for the contrail climate impact, but only effective in the microphysical pathway; in the synoptic pathway the ice crystals sublimate anyway in the subsaturated air. The application of (still expensive and not available in large amounts) alternative fuels for the benefit of climate should thus be planned carefully and it would help to know in advance which contrail termination pathway is more likely in the current or forecast weather situation.

In this paper, we consider the contrail termination pathways from the viewpoint of two time-scales, the sedimentation time-scale τ_{sed} and the synoptic time-scale τ_{syn}. Time-scales are understood as e-folding times, that is, the time span it needs for the process in question to reduce a characteristic contrail-related value (e.g. its ice mass) by e^{-1}. The lifetime of a contrail can be twice or three times the time-scale.. It will turn out that both time-scales are of the same order of magnitude (a couple of hours), which is probably the reason why it is not yet known which pathway dominates globally and climatologically, or if one of them dominates at all.. Perhaps, it could also imply that in many cases neither of the two pathways dominates. However, if in a given situation the aviation weather forecast would result in $\tau_{\mathrm{sed}} < \tau_{\mathrm{syn}}$, then the microphysical pathway is likely, and alternative fuels can effectively be used. On the contrary, if $\tau_{\mathrm{sed}} > \tau_{\mathrm{syn}}$ is predicted, the synoptic pathway will probably dominate, rendering the use of alternative fuels inefficient.

The paper is structured as follows: The data used in the study are described in section Sect. 2. In section Sect. 3 the methods and results of the to determine the time-scale for sedimentation of ice crystals in cirrus and contrails (in section Sect. 3.1) and contrail movements out of ice supersaturated regions (in section Sect. 3.2) are shown. Case studies are presented in Sect. 4. The results are discussed in section Sect. 5. At the end, we conclude in section Sect. 6.

2 Data

Four times per day the German Weather Service (DWD) provides hourly aviation weather forecasts (WAWFOR data), based on the weather forecast model ICON (Zängl et al., 2015). For the present analysis, the temperature and the relative humidity with respect to water (~~RH_w~~ RH_w) are used to calculate the relative humidity with respect to ice (~~RH_i~~ RH_i). In addition, wind data are used, which are given in their zonal and meridional components. Usually, aviation users are informed on temperature, humidity, winds, etc. based on the WAWFOR data ~~inform aviation users about the temperature, humidity, winds, etc.~~ (WAWFOR Package 1). For the German D-KULT project (Demonstrator Klima- und Umweltfreundlicher Lufttransport; Demonstration of climate- and environmentally friendly air transport), additional datasets are produced. They provide information about the potential to form persistent contrails. There is a binary field called the potential of persistent contrails PPC (either 0 or 1). PPC is obtained from the Schmidt-Appleman criterion ~~(SAC)~~ (Schumann, 1996) applying an overall propulsion efficiency of $\eta = 0.365$ and using temperature and relative humidity from the regular forecast. For the compensation of a low humidity bias in the forecast (Gierens et al., 2022), situations with RH_i ~~RH_i~~$> 93\%$ are considered ice (super)-saturated (Hofer et al., 2024). Unfortunately, it is not possible to directly test the sensitivity of the results on these assumptions, since the values are fixed in the system that produces the WAWFOR output. Experience from an earlier test with ICON output (Gierens, 2021) indicates that the appearance of ISSRs does not change very much between thresholds from 90 to 99% in the ICON data. Thus, $PPC = 1$ marks grid points where persistent contrails are possible, ~~and~~ $PPC = 0$ marks all the rest where either no contrails at all or merely short contrails can be formed. The data are available globally and with higher spatial resolution for the European region (EU nest, $0.0625° \times 0.0625°$, approx. $6.5\,\mathrm{km} \times 6.5\,\mathrm{km}$). The latter are used here in an area from $23.5°$W to $62.5°$E and $29.5°$N to $70.5°$N. The WAWFOR data are provided on 57 flight levels which are interpolated from the 120 vertical terrain-following levels of ICON. Flight levels, FL (1 FL corresponds to 100 feet or approximately 60 m), are the usual altitude measure within the aviation community. In WAWFOR, they range from FL 50 (5000 feet altitude) to FL 600 in steps of 10 and include additionally FL 675. We consider the situations at 250 hPa for three days with different weather conditions: 18 April 2024, 01 May 2024 and 24 May 2024 ~~18/04/2024, 01/05/2024, and 24/05/2024~~.

The data for the description of the synoptic situations have been obtained from the Pamore system (DWD, 2024) of DWD. They are based on ICON forecasts as well.

3 Methods and results

3.1 Time-scale for sedimentation of ice crystals in cirrus and contrails

An analytical expression for the time-scale of ice crystal sedimentation from contrails or cirrus clouds can be derived using equations provided by Spichtinger and Gierens (2009, in the following abbreviated SG09).

Let us consider a contrail filling a volume $H \times W \times L$ (height, width, length). Let the ice mass inside this volume be $M = HWL \cdot \varrho q_i$ (with air density ϱ and ice mass mixing ratio q_i). The change of M due to sedimentation is given by the sedimentation flux $F_m \times WL$:

$$\left(\frac{dM}{dt}\right)_\mathrm{sed} = HWL\varrho\frac{dq_i}{dt} = WLF_m,$$

$$\text{thus} \qquad H\varrho\frac{dq_i}{dt} = F_m. \tag{1}$$

Now, the flux density F_m is $\varrho q_i v_m$ where v_m is the mass-weighted fall speed of an ensemble of ice crystals. The latter is computed in SG09 via general moments μ_k of the ice crystal mass distribution:

$$v_m = \gamma(m)\mu_{\delta(m)+1}/\mu_1. \tag{2}$$

$\gamma(m), \delta(m)$ are mass-dependent, but piecewise constant. In the range relevant for contrails their values are $\gamma = 63292.4, \delta = 0.57$ (please note that the given value of γ is only valid for SI-units, kg, m, s, see table 2 in SG09). Further, we note that $q_i = \mu_1 = N_i \cdot \overline{m}$, with the crystal number per kg of air N_i and the mean ice crystal mass $\overline{m}$. The other moment required is given as $\mu_{\delta+1} = N_i \cdot \overline{m}^{(\delta+1)} r_0^{(\delta+1)\delta/2}$. Here, r_0 is a parameter that determines the width of the (lognormal) mass distribution (typically $2 \leq r_0 \leq 4$). Thus, $\mu_{\delta(m)+1}/\mu_1 = \overline{m}^{0.57} r_0^{0.45}$.

Finally, we determine the sedimentation time-scale as $\tau_{\text{sed}}^{-1} = (1/q_i) dq_i/dt$ and find by combining the expressions just derived:

$$\tau_{\text{sed}} = \frac{H}{\gamma\,\overline{m}^{0.57} r_0^{0.45}}. \tag{3}$$

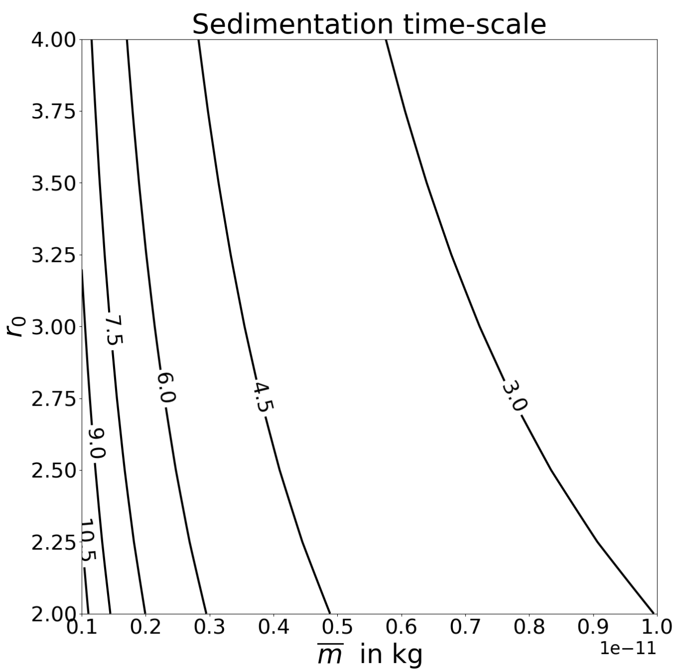

Figure 1. Time-scale for sedimentation of ice crystals out of contrails with ~~height~~ 500 m vertical extension, H, in hours as a function of mean crystal mass $\overline{m}$ and mass distribution width parameter r_0. As the time-scale is proportional to H, ~~contrail height,~~ time-scales for different values of H ~~contrail heights~~ can easily be derived from these curves; for instance, a time-scale of 6 h for an $H = 500$ m would reduce to 3 h for $H = 250$ m. ~~for instance, a time-scale of 5 h for a 500 m deep contrail would reduce to 3 h for a 300 m deep one.~~

Note, that τ_{sed} is in seconds and $\overline{m}$ must be taken in kg (SI-units). For $H = 500\,\mathrm{m}$ and a mean mass of the order $10^{-12}\,\mathrm{kg}$ the sedimentation time-scale is a few hours (say 2.5 to 10 hours, see Fig. 1).

3.2 Contrail movements relative to ice supersaturated regions

3.2.1 Time-scale for contrails to leave an ISSR with the wind in theory

The results below will show that the time span, T, an air parcel resides within an ISSR is Weibull-distributed, that is

$$S(T) = 1 - F(T) = \exp[-(T/T_0)^k]. \tag{4}$$

Here, $S(T)$ is the survival function, and $F(T)$ is the cumulative distribution function of T (see Gierens and Vázquez-Navarro, 2018). For the case of sedimentation, we defined a time-scale as the time span during which ~~time when~~ a fraction of about e^{-1} of the ice mass is still left in the contrail. To be consistent with that definition we define the time-scale, τ_{syn} for leaving an ISSR as that time, where the survival function reaches the same value, $S(\tau_{\mathrm{syn}}) = e^{-1}$. This time is given by the parameter T_0, independently of the exponent k of the Weibull distribution. Our result is thus:

$$\tau_{\mathrm{syn}} = T_0. \tag{5}$$

The Weibull fits in the paper yield straight lines of the form

$$\ln\ln[1/S(T)] = \beta + k\ln(T/T_u) \tag{6}$$

where β is the intercept and k is the slope. T_u is a unit of time, e.g. 1 s. Solving for the survival function and using Eq. 4 yields

$$\tau_{\mathrm{syn}} = T_0 = T_u \exp[-(\beta/k)]. \tag{7}$$

A contour plot showing the synoptic time-scale as a function of β and k is given in Fig. 2.

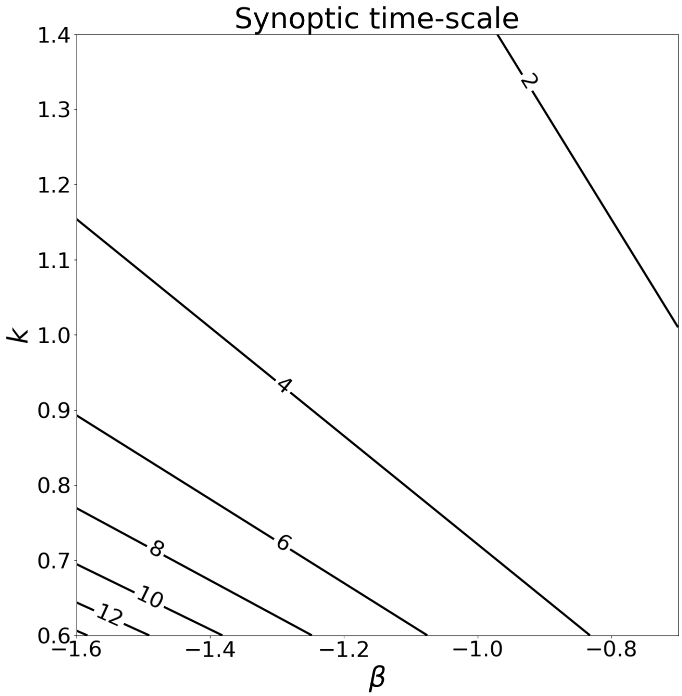

Figure 2. Time-scale for contrails to leave an ISSR (in hours). Small values of τ_{syn} can be reached for small absolute values of β and ~~small~~ large values of k and *vice versa*. Small values of τ_{syn} indicate that the synoptic pathway of contrail dissolution may dominate.

3.2.2 Trajectory calculations and determination of synoptic time-scales

The synoptic time-scales are computed statistically. We consider air parcels at grid points with $PPC = 1$ and determine how long they remain ice supersaturated during a series of WAWFOR forecast times up to 25 h. To this end, we perform trajectory calculations, which are started one hour after the initialisation of the forecast. For each subsequent hour, it is tested whether an initially ice supersaturated air parcel is still supersaturated or not. For this decision, the RH_{i} ~~RHi~~ value of the grid point where the air parcels arrive~~s~~ after one hour (transported by the wind) is used. Air parcels that are still supersaturated are transported further for the next hour, the others are no longer transported. This procedure is repeated until the last forecast step, $+24$ h after starting time~~$+25$ h~~. Initially and at each subsequent time step the number of air parcels which are still supersaturated is recorded. These numbers yield the survival function $S(t)$ (i.e. number of air parcels that are supersaturated at time step t, divided by the number of initially supersaturated air parcels). The statistical analysis of this function provides the desired synoptic time-scale.

However, systematic errors due to the 1 h time step cannot be excluded. Air parcels at the edge of an ISSR could leave and re-enter it within one hour, or even re-enter another ISSR that might be nearby or appear as a new ISSR. This can lead to errors, in particular when ISSRs in the forecast have small-scale structures such that their perimeter-to-area ratio is large. The problem should be small for large continuous ISSRs with little small-scale structure (in the forecast).

4 Case studies

In the following, various examples of the movement of areas with $PPC = 1$ at forecast initialisation are shown under different weather conditions. The following three days are selected: 18 April 2024, 01 May 2024 and 24 May 2024 18/04/2024, 01/05/2024, and 24/05/2024. First, the synoptic weather situation is briefly described for each day. For this, we show maps of the normalised geopotential height Z^*; the normalisation procedure is described in Wilhelm et al. (2022). Normalisation of the geopotential has the advantage of spanning a unique range regardless of the pressure level considered. To this end, each pressure level is assigned a "nominal" geopotential height, and then the actual value of the geopotential height is divided by the nominal value. This results in a small range of values around unity. The These maps show furthermore where the air moves upward (blue) or downward (red) together with the ISSRs (stippling). Then, a series of plots show both the initial $PPC = 1$ region (red outline) and the ISSRs one or more hours later (blue outline); additionally, the plots show with green colour all grid points where the initially supersaturated air parcels (potential persistent contrails) have been transported to and where they survived so far. The green area thus diminishes during the plot series. Finally, the survival function is plotted on the so-called Weibull paper, that is, in a way such that a Weibull distribution appears as a straight line, from which we can determine slope and intercept.

In the first two examples, only the start and end times of the ISSR situations are shown. In the last example, some more steps in between are also shown for illustration purposes.

4.1 Case 1: 18 April 2024

The weather situation on 18 April 2024 (12 UTC) and in the following hours is characterised by a trough in the upper troposphere at high altitudes that begins over Sweden and extends over Germany, Italy and as far as North Africa. This trough is closely linked to the formation of high- and low-pressure regions on the ground. On the back of the trough, the isohypses run closer together and converge. Due to the greater curvature of the isohypses at the southwestern tip of the trough axis, the wind is slowed down. This leads to the air accumulating in front of the trough axis. In order to balance out the excess mass in front of the trough axis, air masses are transported away. Since the tropopause is soon reached above, the air masses are preferentially transported downwards towards the ground. This motion increases the air pressure on the ground and a high-pressure region is formed on the back of the trough. On the front side of the trough, the curvature of the isohypses decreases as they diverge. This leads to a lack of mass, which is compensated by air masses rising from the ground below. This causes the air pressure on the ground to fall and a low-pressure region is created.

The large-scale sinking of air masses on the back of the trough and the rising in the front of the trough can also be seen in Fig. 3: there, on the back of the trough, mainly red areas (sinking), and on the front of the trough mainly blue areas can be seen (rising). Consequently, ice supersaturation occurs on the front side of the trough, in particular at its northeastern edge. It should also be emphasised that ice supersaturation occurs mainly at $Z^* \geq 0.98$.

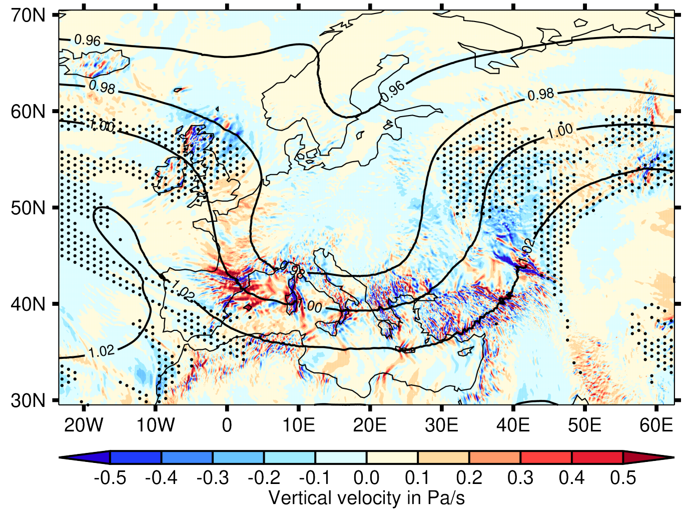

Figure 3. The Synoptic situation for 18 April 2024, at 12 UTC. ~~charts for 18/19 April 2024~~.Shown are the normalised geopotential height (contours), the vertical velocity (in pressure coordinates), and the ISSRs (stippling) at 250 hPa.

In Fig. 4 the $PPC = 1$ region at start time (18 April 2024, from the forecast of 12 UTC + 1 h) is shown as the red contours in both panels. The blue contours show the ISSRs one hour later on the left and 24 hours later on the right panel. The green colour shows the initial $PPC = 1$ grid points that are still inside ISSRs, that is, they are all within the blue contours. After one hour there are still about 75% of the ~~many~~ green points, but 24 hours later only very few ($< 1\%$) green points are still present.

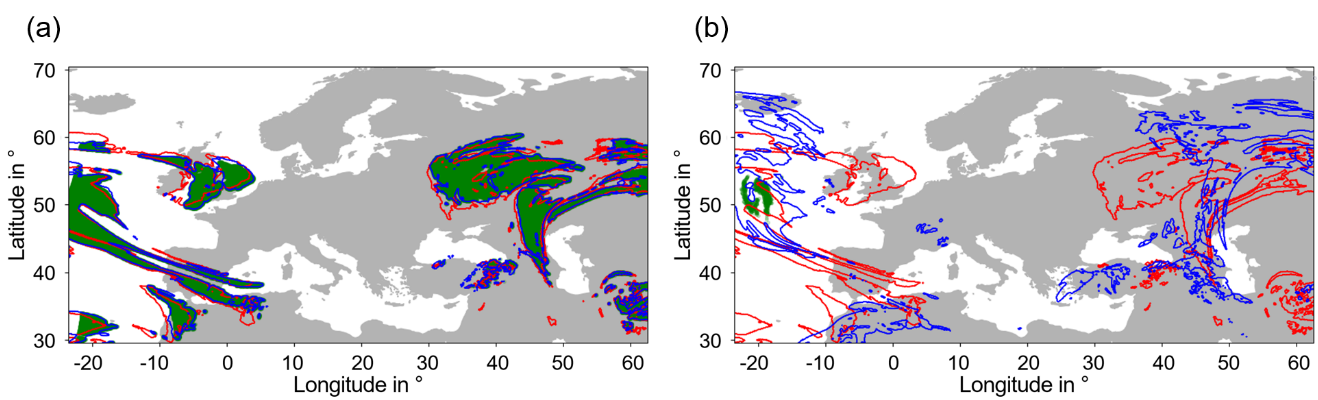

Figure 4. $PPC = 1$ regions (red contours) at the beginning (18 April 2024, from the forecast of 12 UTC + 1 h) at 250 hPa in both panels, the ISSRs (blue contours) in the following hour (in the left panel) and 24 hours after the beginning (in the right panel). The green colour shows the initial $PPC = 1$ grid points that are still inside ISSRs.

Figure 5 shows the survival function of the number of grid points that were initially within $PPC = 1$ regions and that stayed continuously within ISSRs together with the best linear fit on the Weibull paper. The fit can reproduce the curve very well and only deviates slightly towards the end for large values of T, where the statistics get worse because the number of surviving air parcels gets smaller and smaller with increasing T. ~~where the curve begins to fluctuate due to noise.~~ For this case, we determine a slope of $k = 0.9$ and an intercept $\beta = -1.1$. According to Fig. 2 , this implies a time-scale of approximately 4 hours.

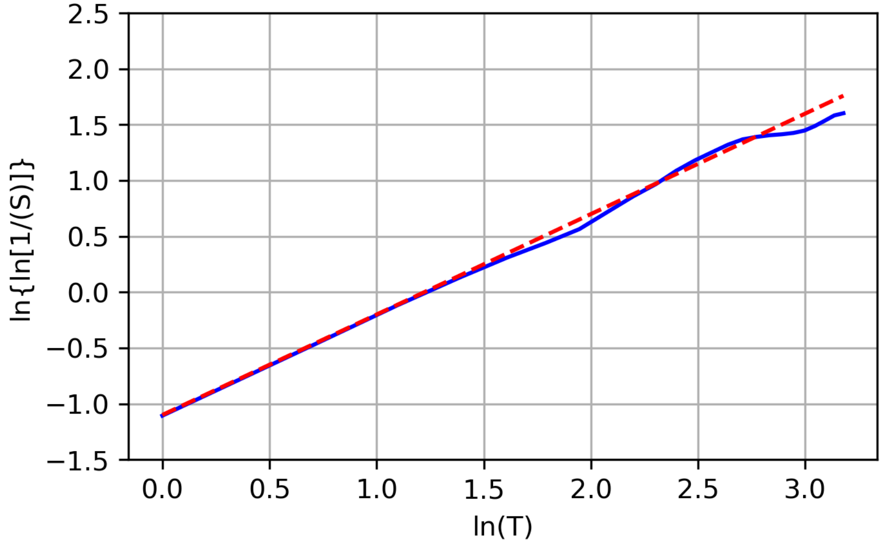

Figure 5. Survival function of the number of grid points that were initially within $PPC = 1$ regions and that survive by always being recorded within an ISSR in the following hours (blue) plotted on Weibull paper together with a linear fit as a dashed line: $g = 0.9 \cdot x - 1.10$ (red).

4.2 Case 2: 1 May 2024

The synoptic situation on 1 and 2 May 2024 is primarily determined by the wedge~~,~~ which stretches from the Mediterranean Sea off the coast of Libya and Egypt across Turkey, Poland~~,~~ and Scandinavia to the northern coast of the United Kingdom (see Fig. 6). Also in this case, ice supersaturation mainly exists for $Z^* \geq 0.98$ in areas with upward air movement.

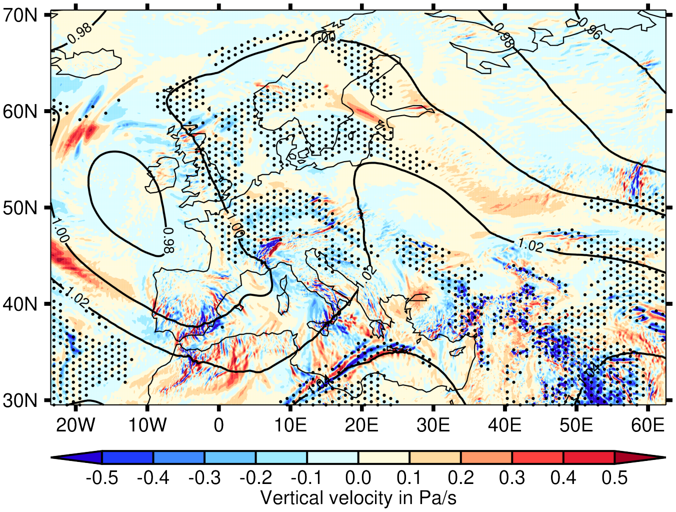

Figure 6. Synoptic situation for 1 May 2024 at 12 UTC. ~~charts for 01/02 May 2024~~.Shown are the normalised geopotential height (contours), the vertical velocity (in pressure coordinates) and the ISSRs (stippling) at 250 hPa.

Figure 7 shows the $PPC = 1$ region at start time (1 May 2024, from the forecast of 12 UTC + 1 h) as the red contours in both panels. The blue contours show the ISSRs one hour later on the left and 24 hours later on the right panel. The green colour shows the initial $PPC = 1$ grid points that are still inside ISSRs. After one hour there are still many green points (about 71% survive), but after 24 hours almost all (99.8%) have vanished.

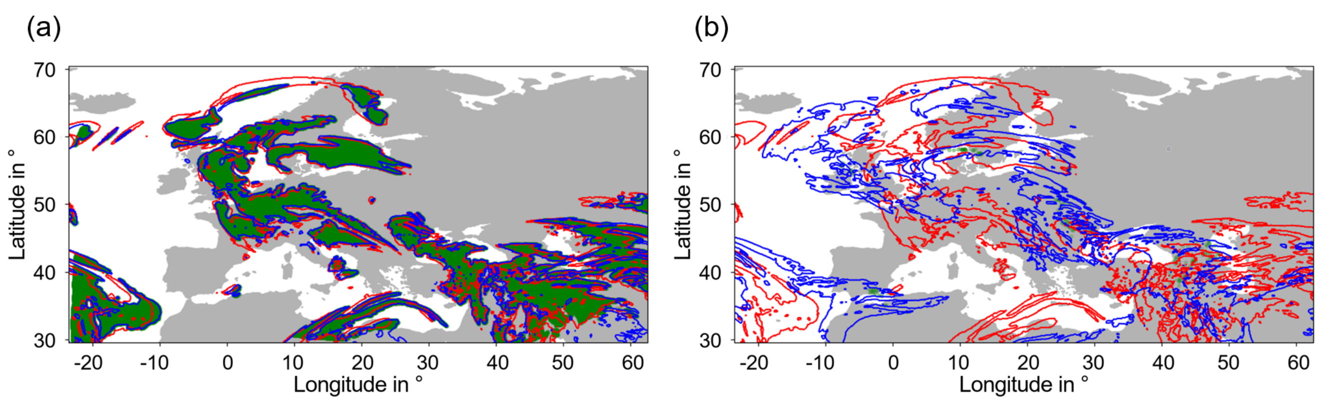

Figure 7. $PPC = 1$ regions (red contours) at the beginning (1 May 2024 from the forecast of 12 UTC + 1 h) at 250 hPa in both panels, the ISSRs (blue contours) on the following hour (in the left panel) and 24 hours after the beginning (in the right panel). Green colour shows the initial $PPC = 1$ grid points that are still inside ISSRs.

The survival function for this case can ~~excellently~~ be fitted with a Weibull distribution with a slope of $k = 0.92$ and an intercept $\beta = -1.09$, see Fig. 8. The synoptic time-scale is thus again about 4 h.

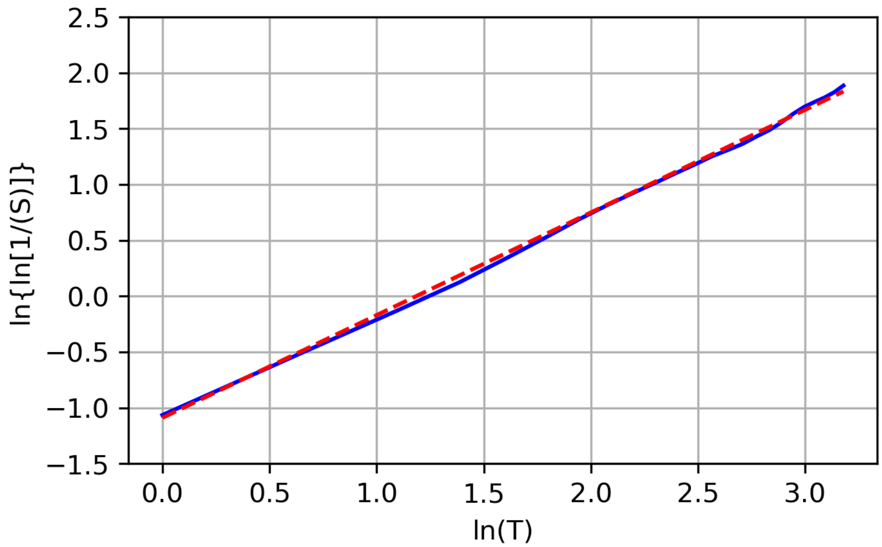

Figure 8. Survival function of the number of grid points that were initially within $PPC = 1$ regions and that survive by always being recorded within an ISSR in the following hours (blue) plotted on Weibull paper together with a linear fit as a dashed line: $g = 0.92 \cdot x - 1.09$ (red).

4.3 Case 3: 24 May 2024

This situation (see Fig. 9) is characterised by ~~exclusively~~ high values of the normalised geopotential height throughout the considered region and also large areas with ice supersaturation over Scandinavia, Russia, Central Europe, Iran, Libya~~,~~ and Egypt, which occurs mainly in raising air at $Z^* > 1.0$.

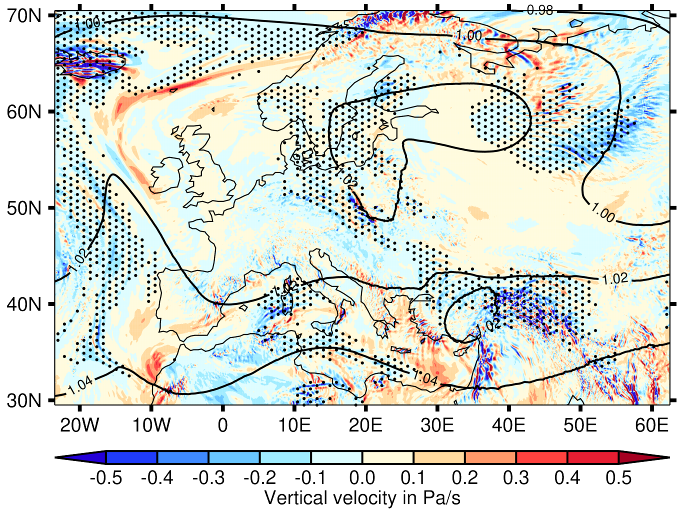

Figure 9. Synoptic situation for 24 May 2024 at 12 UTC ~~charts for 24/25 May 2024~~. Shown are the normalised geopotential height (contours), the vertical velocity (in pressure coordinates) and the ISSRs (stippling) at 250 hPa.

Figure 10 shows the evolution of the surviving initial contrail grid points in more detail, that is, with more intermediate time steps. The $PPC = 1$ regions at start time (24 May 2024, from the forecast of 12 UTC + 1 h) are again shown as the red contours in all panels. The blue contours show the ISSRs 1 hour (a), 3 hours (b), 5 hours (c), 10 hours (d), 15 hours (e) and 24 hours (f) later. The green colour shows as usual the initial $PPC = 1$ grid points that are still inside ISSRs at the respective time steps. The number of green points decreases continuously over time. After one hour, about 76% of the air parcels are still supersaturated, but after 24 hours less than 0.1% survive.

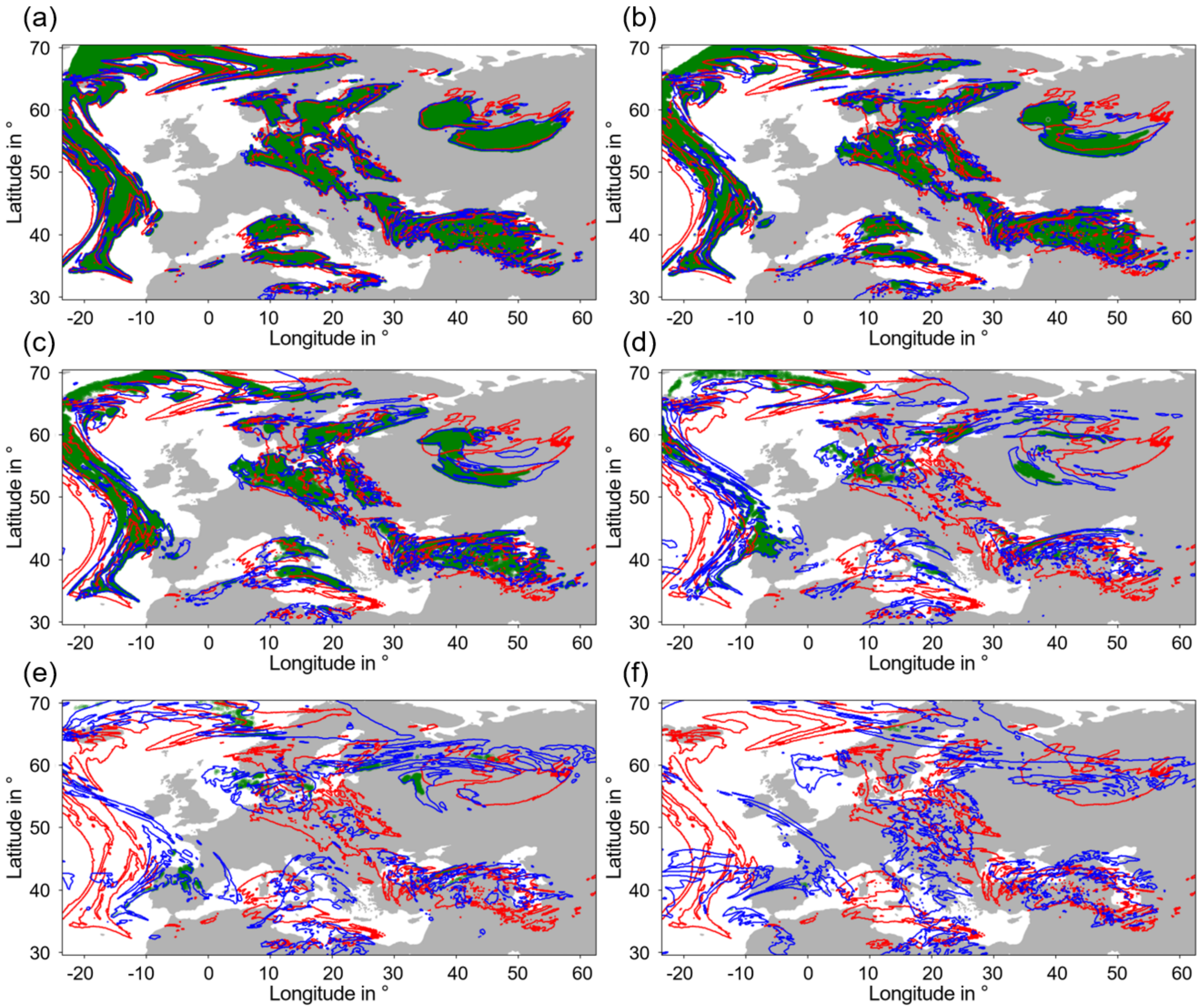

Figure 10. All panels show the $PPC = 1$ regions at the beginning (24 May 2024 from the forecast of 12 UTC + 1 h) at 250 hPa as red contours. The six different panels indicate ISSRs from a selection of the following hours in blue (horizontally from top left to bottom right: ISSRs 1 h later at 12 UTC + 2 ~~hrs~~ h; ISSRs 3 ~~hrs~~ h later; ISSRs 5 ~~hrs~~ h later; ISSRs 10 ~~hrs~~ h later; ISSRs 15 ~~hrs~~ h later and ISSRs 24 ~~hrs~~ h later). Grid points that were within ice supersaturation in every subsequent hour since the beginning are marked in green.

Figure 11 shows the survival function for this case. The best Weibull fit for this case has a slope of $k = 1.02$ and an intercept $\beta = -1.30$. This is nearly an exponential distribution (which would have $k = 1$). The corresponding time-scale is again about 4 hours.

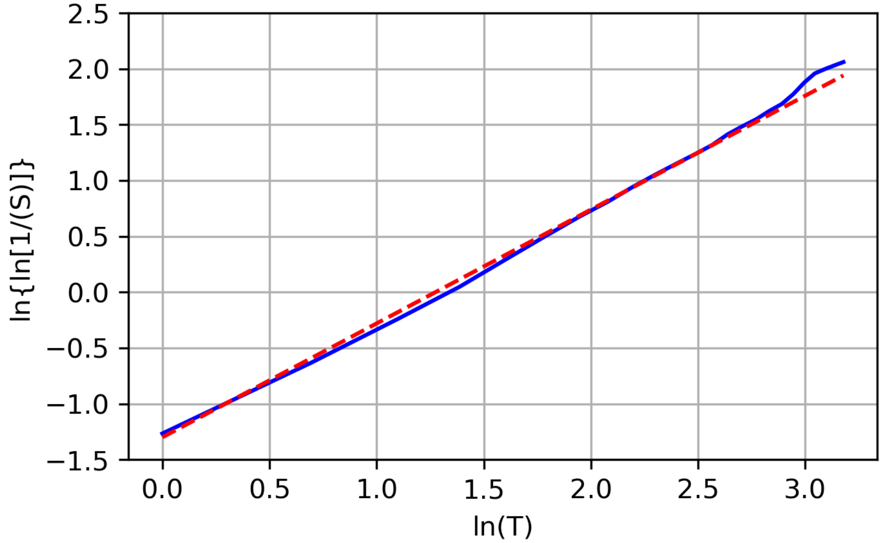

Figure 11. Survival function of the number of grid points that were initially within $PPC = 1$ regions and that survive by always being recorded within an ISSR in the following hours (blue) plotted on Weibull paper together with a linear fit as a dashed line: $g = 1.02 \cdot x - 1.30$ (red).

5 Discussion

5.1 Seasonal and geographical variability

The three case studies have been performed for ISSRs in a certain season (spring 2024) over a certain geographical region (Europe and the western North-Atlantic). The resulting synoptic time-scales may thus lack generality and may vary if other seasons and other geographical regions are considered. ISSRs may vary in horizontal extension and their own lifetime, due to the prevalent synoptic situations in different parts of the world. Unfortunately, there is not much known about these issues, since ISSRs cannot be observed directly. But there are at least indirect indications, for instance the so-called potential contrail coverage (ISSRs where the thermodynamic contrail formation criterion is fulfilled, Sausen et al., 1998) and the path length distribution of aircraft which cross ISSRs (Spichtinger and Leschner, 2016). The potential contrail coverage is larger over the USA and south-east Asia than over Europe and the North-Atlantic (Sausen et al., 1998). Path lengths through ISSRs are on average larger in the extra tropics than in the tropics (Spichtinger and Leschner, 2016), but the path length distributions overlap substantially. In the extra tropics, path lengths are larger in fall and winter than in spring and summer, in the tropics the seasonal differences are smaller. In any case, due the the strongly skewed path length distributions, the geographical and seasonal differences are much smaller than the standard deviations of the distributions. Variations in potential contrail coverage and path lengths may imply corresponding variations in the synoptic time-scales. But the large variability, that is indicated in the path length distributions, may imply that these variations are statistically insignificant.

4.1 Time-scales and lifetimes

It is important to distinguish time-scales from lifetimes. The lifetime of a contrail can be defined as the period from its formation until it can no longer be seen or until some other threshold is underrun. In principle, such a period can precisely be determined, although this is in most cases not required. In contrast, a time-scale is rather understood as a rough estimate than a precise value. It is the time that it takes for a considerable (another vague word) change to a system, for instance, an e-folding time. (This does not exclude the possibility of giving precise e-folding times, for instance for radioactive decay). If we take a time-scale as an e-folding time, for instance, for the loss of ice mass, a corresponding lifetime would be twice or three times as long (as $e^{-2} \approx 0.14$ and $e^{-3} \approx 0.05$). One should also note that factors of the order one are unimportant for time-scale considerations. For instance, the shrinking of ice crystals can be considered via the reduction of its mass or its radius. Although the same process is considered, the corresponding time-scales differ by approximately a factor of three (for spherical crystals).

It follows from these considerations that it is not necessary to put very much effort into the numerical determination of the synoptic time-scale. In our view, the calculation of trajectories in the horizontal dimension with a simple Euler-forward method and the application of the nearest neighbour approach to map relative humidity values to trajectory locations after each time step is sufficient for the estimation of a time-scale.

However, some systematic errors cannot be excluded. When calculating the synoptic time-scale for contrails to leave their parent ISSR, we only have 1-hour time steps. One cannot determine whether an air parcel resided always inside the ISSR during this hour. Air parcels at the edge of an ISSR could leave and re-enter it within one hour, or even re-enter another ISSR that might be nearby or appear as a new ISSR. This can lead to errors, in particular when ISSRs in the forecast have small-scale structures such that their perimeter-to-area ratio is large. The problem should be small for large continuous ISSRs with little small-scale structure (in the forecast).

At the start of the trajectory calculations, the ISSRs are already present and have already an age, that can exceed a day. One might believe that this leads to an underestimation of the synoptic time-scale, but we do not think so. Had we tried to determine a lifetime of ISSRs, then this could be a source of error. But here we are concerned with the time it needs for an air parcel to leave an ISSR due to the differences in the motion of the wind and the motion of the ISSR (Hofer and Gierens, 2025). We do not see how this time-scale could be biased by the fact that the ISSRs have already some age at the beginning of our calculations.

5.2 Comparison with results from the literature

The results obtained in our case studies all gave Weibull-type survival functions, with parameters β slightly below -1 and k between 0.9 and about 1. The corresponding synoptic time-scales are close to 4 hours in all three cases. We can compare these results with results from the literature.

Let us first mention that contrail lifetimes obtained from a study using satellite-tracking of contrails (Gierens and Vázquez-Navarro, 2018) gave a mean lifetime of $3.7\,\mathrm{h}$ which is consistent with both the synoptic and the sedimentation time-scales derived in this study (although the comparison is a little off since the mean of a Weibull distribution differs from its scale parameter). Unfortunately, the satellite-tracking cannot distinguish whether a contrail disappeared due to sedimentation of its crystals or due to sublimation in dry air, in particular, as the late contrail evolution can often not be observed in satellite images due to vanishing contrast. To determine the mean lifetimes in the satellite study, the authors applied statistical arguments and modelling, based on the Weibull distribution, which provided a good fit to the observed survival function. The parameters in that study lead to a quite short time-scale of about 0.6 h, a consequence and indication of the fact that only a part of the contrail lifetime can be observed via satellite-tracking.

A direct comparison is possible with the results of trajectory calculations presented by Dietz (2012). He uses NWP data from the COSMO model version that was operational in 2012. This was equipped with a 1-moment microphysics scheme. Furthermore, he uses a non-operational version with a 2-moment scheme (Seifert et al., 2012). The resulting survival functions are fitted with Weibull distributions, as in the present study. ~~An immediate comparison is possible with results from trajectory calculations presented by Dietz 2012. He uses NWP data obtained from the operational version of the COSMO-Model (the model that was operational at DWD at that time, including a one-moment microphysics scheme) and from a non-operational version with a 2-moment scheme (Seifert et al., 2012) and applies fits of Weibull distributions to the survival functions as well.~~ Additionally, two versions of trajectories are calculated: 1) trajectories from the model data (that is, affected by all processes implemented in the model) and 2) a version where the effects of microphysics are switched off. This means, that condensation, sedimentation and precipitation are switched off. This conserves ~~by conserving~~ the initial absolute humidity in the ~~calculation~~idealised simulations (which in reality is reduced by cloud formation) to obtain a "virtual" relative humidity. The following time-scales are determined (k-values in brackets):

- 1-moment scheme: 3.0 hours ($k = 0.9$);
- 2-moment scheme: 3.8 hours ($k = 0.75$);
- 1-moment scheme, virtual "RH_{i}" ~~RHi~~: 4.0 hours ($k = 0.75$);
- 2-moment scheme, virtual "RH_{i}" ~~RHi~~: 5.6 hours ($k = 0.875$).

Two observations are immediately possible: first, the 2-moment scheme leads to longer time-scales, and second, the virtual humidity fields have longer time-scales than the real humidity fields. ~~We think~~ This can be explained quite easily. The 2-moment scheme allows higher ice supersaturation to be obtained in the NWP model than the 1-moment scheme. Thus, ISSRs in the 2-moment schemes have on average higher maximum humidities and it takes longer for them to dry out than for the 1-moment scheme. Switching off microphysics, that is in particular switching off sedimentation of ice crystals, leads again to longer time-scales in both model versions. These two time-scales are ~~probably~~ those that are most directly comparable to the ones that we derived here. Indeed, as our trajectories are based on ICON equipped with a 1-moment model, the synoptic time-scales are equal: 4 hours. We note, however, that our k-values are slightly larger than those obtained by Dietz (2012). This difference might result from methodical differences between our study and that of Dietz (for instance, he used 3-dimensional trajectories, calculated with a Runge-Kutta method; our approach was simpler with a 2-dimensional Euler-forward method).

Numerical simulations of contrails, either with cloud-resolving models (e.g. Unterstrasser and Gierens, 2010a, b; Lewellen, 2014) or with global circulation models (e.g. Bier et al., 2017), provide information on contrail dissolution processes as well. Cloud-resolving simulations usually assume constant synoptic conditions such that contrail dissolution is then only possible via microphysical processes. But it is not only sedimentation that occurs then. Depositional growth of ice crystals reduces the supersaturation in the contrail-containing ISSRs, but it does not lead to subsaturation. Thus, crystal loss in this case is still dominated by sedimentation. Unterstrasser and Gierens (2010a) observe in their simulations fallstreaks developing after 6500 s (1.8 h), but these consist only of very few large crystals. Most of the contrails cease to grow in mass after 3-4 hours when sedimentation and crystal growth (in a constant supersaturation field) balance. Without synoptic evolution, the total extinction first grows and then, after about 3 h, it stagnates or begins to decline, which is due to sedimentation. The authors consider the 3 hours an intrinsic time-scale for contrails, where "intrinsic" means that it is determined by microphysics rather than synoptic evolution. All the sensitivity studies in Unterstrasser and Gierens (2010b) show the same 3 hours intrinsic time-scale. Lewellen (2014) often finds contrails with lifetimes exceeding 10 h. This may seem quite high, but it is within the range of time-scales derived here. Synoptic changes that would lead a contrail into subsaturated environments are not simulated, and the thickness ~~height~~ of the supersaturated layer is assumed to range from 500 to 1500 m. As the author simulates contrails up to their complete demise, contrail lifetimes can be quite long. For comparison, with a height of 1000 m, the time-scales shown in ~~our~~ Figure 1 must be doubled. Since these are e-folding times, the total lifetimes can easily be two or three times as long. Thus ~~we find~~ there is no contradiction between the present and Lewellen's results.

The simulation with a global circulation model, ~~that~~ which for the first time (to our knowledge) introduced the distinction between the microphysical and the synoptic pathway to contrail dissolution, was that of Bier et al. (2017). These authors also mentioned precipitation (aggregation of ice crystals to snow-flakes which fall) and the mixing with ambient natural cirrus (or replacement of contrail cirrus by natural cirrus) as contrail terminating processes, however with considerably smaller effect than sedimentation and synoptic drying. In the study, large contrail clusters are formed on several days and their evolution is observed. In the eight considered cases, sedimentation dominates contrail dissolution in three cases, and synoptic drying in two. The remaining three cases are transition cases (probably cases with $\tau_{\rm sed} \approx \tau_{\rm syn}$). Although the lifetimes of a contrail cluster are not simply comparable to the time-scales considered here, we can see from their figures that several properties of the clusters change at a high rate during the first few hours, but then, after about 5 to 8 hours, further changes are weak. All cases show this behaviour and ~~we think,~~ this suggests that both time-scales should be of the order of 5-8 hours, consistent with our results. Bier et al. (2017) study as well the effect of a reduction of the initial ice crystal number in the contrails, e.g. due to alternative fuels. This leads to larger ice crystal masses and thus, according to Eq. 3 to a shorter sedimentation time-scale. Accordingly, all simulations with reduced ice crystal numbers show shorter contrail lifetimes. Interestingly, the contrail lifetimes are also reduced in the dynamically controlled cases. ~~We think~~ The explanation for this is probably that in the simulations both processes occur simultaneously and sedimentation is active in dynamically controlled cases as well.

As both processes, sedimentation and synoptic evolution, occur simultaneously in nature, the combined time-scale is half the harmonic mean of the two time-scales, because:

$$\frac{1}{\tau} = \frac{1}{\tau_{\rm sed}} + \frac{1}{\tau_{\rm syn}}, \qquad \text{thus} \tag{8}$$
$$\tau = \frac{\tau_{\rm sed}\tau_{\rm syn}}{\tau_{\rm sed}+\tau_{\rm syn}}$$

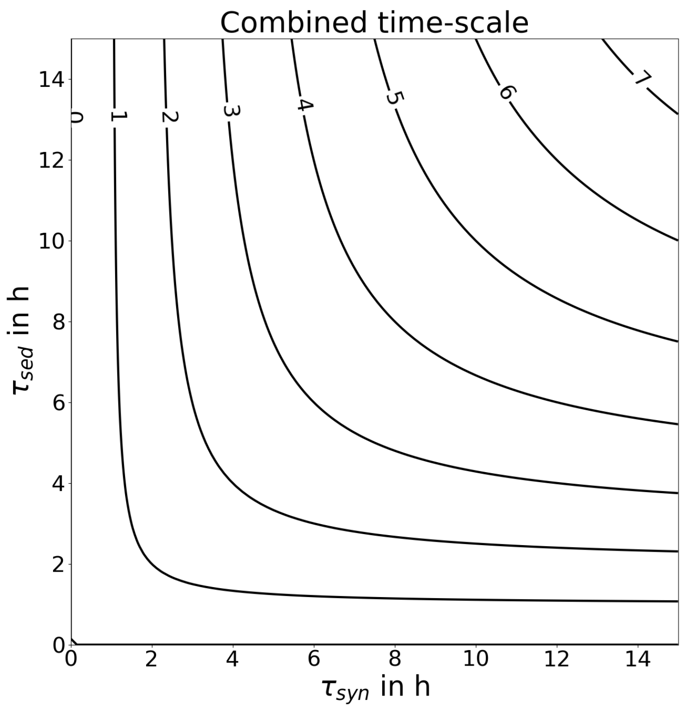

Figure 12. The combined time-scale of $\tau_{\rm sed}$ and $\tau_{\rm syn}$ in hours calculated according to Eq. 8.

The combined time-scale is thus shorter than the two time-scales in separation, see Fig. 12 . It is also shorter than the smaller one of the two time-scales. Even if both time-scales would be ten hours, the combined one is only five hours, which is plausible, since two processes act simultaneously to dissolve the contrail. This explains probably why the satellite observations give shorter time-scales than the cloud-resolving simulations which typically assume constant synoptic conditions and horizontally periodic boundary conditions.

Furthermore, model simulations allow to follow a process up to the very end simply by looking at the output values. In contrast, it is difficult in nature to follow a contrail until complete dissolution. This holds for all methods, for satellite imagery, in-situ measurements with research aircraft and ground observations. Finally, in a model one has the whole ISSR at hand, that is, one can determine its area, volume, ice, and water vapour content, etc. Likewise, if a cloud or contrail is modelled, its properties are in principle completely knowable. This is not possible in nature, neither for ISSRs nor for clouds and contrails. These issues render the comparison of measured and modelled results difficult.

5.3 ISSRs in the synoptic situation

The synoptic weather charts shown to describe the three cases display the normalised geopotential height, Z^*, instead of the geopotential *per se*. This quantity has been introduced by Wilhelm et al. (2022) to make variations of this field comparable, i.e. to bring them on a common scale for different pressure levels. This scale ranges from about 0.9 to about 1.1, independent of pressure in the upper troposphere. Wilhelm et al. (2022) already pointed out that regions, where persistent contrails can form, are characterised by high values of Z^*. This finding is corroborated by the current results: in case 1 there are very few (< 10 grid boxes that have ice supersaturation at $Z^* < 0.98$. Otherwise, ice supersaturation occurs exclusively where $Z^* > 0.98$. In cases 2 and 3, there is no ice supersaturation at all where $Z^* < 0.98$. ~~we find ISSRs (stippling) mainly where $Z^* > 0.98$. In contrast, ISSRs are rarely found where $Z^* < 0.98$.~~ Of course, ISSRs and regions with $Z^* > 0.98$ are not identical. That implies that for contrail avoidance it is still necessary to predict ice supersaturation. But the fact that ISSRs are hardly present in regions with $Z^* < 0.98$ renders the prediction work easier. In such regions it is not necessary to think about contrail prevention, they will hardly persist if they form at all. Calculating Z^* from the normal geopotential height involves the call of one simple function, but this very simple step could save a lot of interpretation work later in flight planning.

This result could only be obtained by normalising the geopotential. Had we not normalised it, the boundary that corresponds to $Z^* = 0.98$ would appear at different heights in different pressure altitudes and it would be difficult to notice that there is such a boundary at all.

6 Conclusion

Contrails are dissolved mainly by the following processes:

- Sedimentation of the ice crystals into lower levels that are subsaturated;
- The (horizontal) wind blows the ice crystals out of the parent ISSRs;
- Large-scale subsidence diminishes supersaturation down to subsaturation.

The first of these processes can be characterized by a sedimentation time-scale, $\tau_{\rm sed}$, which is proportional to the height of the supersaturated layer and which depends weaker than linearly on the mean mass of the contrail ice crystals. Typical values are a couple of hours.

The other two processes can together be characterized by a synoptic time-scale, $\tau_{\rm syn}$, which does not depend on characteristics of the contrail or its ice crystals but only on the large-scale synoptic situation and in particular the relative motion of the parent ISSR and the local wind (see Hofer and Gierens, 2025). The synoptic time-scale is also on the order of a couple of hours. We note however, that the analysis of the current paper involves only three case studies for ice supersaturated regions in two spring months over a region in the northern midlatitude, mainly Europe and the western North-Atlantic. Synoptic situations that are prevalent in spring over this region thus shape the resulting Weibull distributions and in turn, determine the resulting synoptic time-scale. It may well be that these results would be different in other seasons and in other regions of the world where the synoptic circumstances differ from those over the North-Atlantic and Europe. As the sizes of ice supersaturated regions vary seasonally and geographically (Sausen et al., 1998; Spichtinger and Leschner, 2016), the synoptic time-scale is expected to vary as well. Whether it varies simply in proportion to the mean size of ISSRs is unknown.

The fact that both time-scales are similar may explain ~~that~~ why it is unknown whether the microphysical or the synoptic pathway dominates in contrail dissolution. But it can ~~as well~~ also imply that often both pathways are of similar importance.

As other contrail-removing processes are of minor importance, it is the combination of the two time-scales that characterises the lifetime of contrails. This combination is half the harmonic mean of the two time-scales in separation, which is always less than the smaller of the two time-scales. The time-scales in the current paper are defined as e-folding times. Total lifetimes are perhaps rather 2 or three e-folding times.

Cloud-resolving models of contrails usually assume constant synoptic conditions and, applying periodic boundary conditions, effectively assume horizontally infinitely extended ISSRs. Thus, the synoptic time-scale is effectively infinite. Contrail lifetimes in these models are often quite long ($> 10\,\mathrm{h}$). In contrast, contrail simulations in global circulation models where both pathways are effective yield shorter contrail lifetimes (say, about $5-8\,\mathrm{h}$). Both pathways are also effective in nature. ~~the real world.~~ Contrail tracking studies using satellite imagery find thus short lifetimes of the order $4\,\mathrm{h}$.

The sedimentation time-scale of a contrail can be diminished if alternative fuels with reduced soot emission (by number) are applied, as long as the reduction does not lead ~~in~~to the so-called soot-poor regime (that is, where the soot emission index would fall below 10^{13-14} soot particles per kg of fuel, see Kärcher and Yu, 2009). Less soot implies less but larger ice crystals (i.e. with higher mean mass). Thus, the microphysical time-scale can be reduced by technical means, whereas the synoptic time-scale is given by the weather situation. To be an effective means of contrail mitigation, the resulting sedimentation time-scale must be smaller than the synoptic time-scale. In order to determine this in the flight planning phase, trajectory calculations would be necessary. There are currently already services for contrail avoidance in place or under development (e.g. Engberg et al., 2025), which use trajectory calculations to compute the advection of a contrail with the wind. If they represent ice crystal sedimentation in a reliable way the preflight estimation of the two time-scales should in principle be possible.

Finally, a side result of this study is that contrails will hardly persist in regions where the normalised geopotential height, as defined by Wilhelm et al. (2022), is less than 0.98. This simple boundary can easily be calculated for the upper troposphere and we recommend strongly that aviation weather forecasts use normalised geopotential height on their synoptic charts because this allows flight planners to see immediately where contrail prevention actions are not necessary. Note, however, that Wilhelm et al. (2022) derived their statistics from flight data obtained in the northern mid latitudes. It is not known whether this simple result can be generalised to, for instance, more tropical regions. Anyway, most air traffic occurs currently in the northern mid latitudes and for this region, the recipe should be applicable.

Code availability. Python codes can be shared on request.

Data availability.

Author contributions. This paper is part of SH's PhD thesis. SH wrote the codes, ran the calculations, analysed the results and produced the figures. KG supervises her research. Both authors discussed the methods and results and wrote the paper.

Competing interests. The authors declare no competing interests.

Acknowledgements. This research contributes to and is supported by the project D-KULT, Demonstrator Klimafreundliche Luftfahrt (Förderkennzeichen 20M2111A), within the Luftfahrtforschungsprogramm LuFo VI of the German Bundesministerium für Wirtschaft und Klimaschutz. This work used resources of the Deutsches Klimarechenzentrum (DKRZ) granted by its Scientific Steering Committee (WLA) under project ID bd1357. The authors would like to thank Simon Kirschler for his thorough reading and commenting a draft manuscript.

References

Bier, A., Burkhardt, U., and Bock, L.: Synoptic control of contrail cirrus lifecycles and their modification due to reduced soot number emissions, J. Geophys. Res., 122, 11 584–11 603, https://doi.org/10.1002/2017JD027011, 2017.

Dietz, S.: Untersuchung charakteristischer Lebenszyklen von eisübersättigten Regionen in der oberen Troposphäre, Master's thesis, Universität Innsbruck, 2012.

DWD: PArallel MOdel data REtrieve from Oracle databases, last access December 2024, https://www.dwd.de/DE/leistungen/pamore/pamore.html, 2024.

Engberg, Z., Teoh, R., Abbott, T., Dean, T., Stettler, M. E. J., and Shapiro, M. L.: Forecasting contrail climate forcing for flight planning and air traffic management applications: the CocipGrid model in pycontrails 0.51.0, Geoscientific Model Development, 18, 253–286, https://doi.org/10.5194/gmd-18-253-2025, 2025.

Gierens, K. and Vázquez-Navarro, M.: Statistical analysis of contrail lifetimes from a satellite perspective, Meteorol. Z., 27, 183–193, https://doi.org/10.1127/metz/2018/0888, 2018.

Gierens, K., Wilhelm, L., Hofer, S., and Rohs, S.: The effect of ice supersaturation and thin cirrus on lapse rates in the upper troposphere, Atmos. Chem. Phys., 22, 7699–7712, https://doi.org/10.5194/acp-22-7699-2022, 2022.

Gierens, K. M.: Contrail Statistics, Big Hits and Predictability, in: RAeS Conference: Mitigating the climate impact of non-CO2 – Aviation's low-hanging fruit, https://elib.dlr.de/141532/, 2021.

Haywood, J., Allan, R., Bornemann, J., Forster, P., Francis, P., Milton, S., Rädel, G., Rap, A., Shine, K., and Thorpe, R.: A case study of the radiative forcing of persistent contrails evolving into contrail-induced cirrus, J. Geophys. Res., 114, D24 201, https://doi.org/10.1029/2009JD012650, 2009.

Hofer, S. and Gierens, K.: Kinematic properties of regions that can involve persistent contrails, EGUsphere, 2024, 1–23, https://doi.org/10.5194/egusphere-2024-3520, 2025.

Hofer, S., Gierens, K., and Rohs, S.: How well can persistent contrails be predicted? — An update, Atmos. Chem. Phys., 24, 7911—-7925, https://doi.org/10.5194/acp-24-7911-2024, 2024.

Kärcher, B. and Yu, F.: Role of aircraft soot emissions in contrail formation, Geophys. Res. Lett., 36, L01 804, doi:10.1029/2008GL036 694, 2009.

Lewellen, D.: Persistent Contrails and Contrail Cirrus. Part II: Full Lifetime Behavior, J. Atmos. Sci., 71, 4420–4438, https://doi.org/10.1175/JAS-D-13-0317.1, 2014.

Minnis, P., Young, D., Nguyen, L., Garber, D., Jr., W. S., and Palikonda, R.: Transformation of contrails into cirrus clouds during SUCCESS, Geophys. Res. Lett., 25, 1157–1160, 1998.

Moore, R. H., Thornhill, K. L., Weinzierl, B., Sauer, D., D'Ascoli, E., Kim, J., Lichtenstern, M., Scheibe, M., Beaton, B., j. Beyersdorf, A., Bulzan, D., Corr, C. A., Crosbie, E., Jurkat, T., Martin, R., Riddick, D., Shook, M., Slover, G., Voigt, C., White, R., Winstead, E., Yasky, R., Ziemba, L. D., Brown, A., Schlager, H., and Anderson, B. E.: Biofuel blending reduces particle emissions from aircraft engines at cruise conditions, Nature, 543, 411–415, https://doi.org/10.1038/nature21420, 2017.

Sausen, R., Gierens, K., Ponater, M., and Schumann, U.: A diagnostic study of the global distribution of contrails, Part I. Present day climate, Theor. Appl. Climatol., 61, 127–141, 1998.

Schumann, U.: On conditions for contrail formation from aircraft exhausts, Meteorol. Z., 5, 4–23, 1996.

Schumann, U., Mayer, B., Graf, K., and Mannstein, H.: A parametric radiative forcing model for contrail cirrus, J. Appl. Meteorol. Climatol., 51, 1391–1406, 2012.

Schumann, U., Penner, J. E., Chen, Y., Zhou, C., and Graf, K.: Dehydration effects from contrails in a coupled contrail–climate model, Atmos. Chem. Phys., 15, 11 179–11 199, https://doi.org/10.5194/acp-15-11179-2015, 2015.

Seifert, A., Köhler, C., and Beheng, K.: Aerosol-cloud-precipitation effects over Germany as simulated by a convective-scale numerical weather prediction model, Atmos. Chem. Phys., 12, 709–725, https://doi.org/10.5194/acp-12-709-2012, 2012.

Spichtinger, P. and Gierens, K.: Modelling of cirrus clouds — Part 1a: Model description and validation, Atmos. Chem. Phys., 9, 685–706, 2009.

Spichtinger, P. and Leschner, M.: Horizontal scales of ice-supersaturated regions, Tellus B: Chemical and Physical Meteorology, 68, 29 020, https://doi.org/10.3402/tellusb.v68.29020, 2016.

Sussmann, R. and Gierens, K.: Differences in early contrail evolution of 2–engined versus 4–engined aircraft. Lidar measurements and numerical simulations, J. Geophys. Res., 106, 4899–4911, 2001.

Unterstrasser, S. and Gierens, K.: Numerical simulations of contrail-to-cirrus transition – Part 1: An extensive parametric study, Atmos. Chem. Phys., 10, 2017–2036, 2010a.

Unterstrasser, S. and Gierens, K.: Numerical simulations of contrail-to-cirrus transition – Part 2: Impact of initial ice crystal number, radiation, stratification, secondary nucleation and layer depth, Atmos. Chem. Phys., 10, 2037–2051, 2010b.

Verma, P. and Burkhardt, U.: Contrail formation within cirrus: ICON-LEM simulations of the impact of cirrus cloud properties on contrail formation, Atmos. Chem. Phys., 22, 8819–8842, https://doi.org/10.5194/acp-22-8819-2022, 2022.

Voigt, C., Kleine, J., Sauer, D., Moore, R., Bräuer, T., Clercq, P. L., Kaufmann, S., Scheibe, M., Jurkat-Witschas, T., Aigner, M., Bauder, U., Boose, Y., Borrmann, S., Crosbie, E., Diskin, G., DiGangi, J., Hahn, V., Heckl, C., Huber, F., Nowak, J., Rapp, M., Rauch, B., Robinson, C., Schripp, T., Shook, M., Winstead, E., Ziemba, L., Schlager, H., and Anderson, B.: Cleaner burning aviation fuels can reduce contrail cloudiness, Communications Earth & Environment, 2, 1–10, https://elib.dlr.de/144492/, 2021.

Wilhelm, L., Gierens, K., and Rohs, S.: Meteorological conditions that promote persistent contrails, Appl. Sci., 12, 4450, https://doi.org/10.3390/app12094450, 2022.

Wolf, K., Bellouin, N., and Boucher, O.: Sensitivity of cirrus and contrail radiative effect on cloud microphysical and environmental parameters, Atmos. Chem. Phys., 23, 14 003—-14 037, https://doi.org/10.5194/acp-23-14003-2023, 2023.

Zängl, G., Reinert, D., Ripodas, P., and Baldauf, M.: The ICON (ICOsahedral Non-hydrostatic) modelling framework of DWD and MPI-M: Description of the non-hydrostatic dynamical core, QJRMS, 141, 563–579, https://doi.org/10.1002/qj.2378, 2015.